THRESHOLD CURRENT AND MODULATION RESPONSE OF SEMICONDUCTOR LASERS

BY

GREGORY ALEXANDER KOSINOVSKY

B.S., University of Illinois, 1988
M.S., University of Illinois. 1990

THESIS

Submitted in partial fulfillment of the requirements
for the degree of Doctor of Philosophy in Electrical Engineering
in the Graduate College of the
University of Illinois at Urbana-Champaign, 1995

Urbana, Illinois

UNIVERSITY OF ILLINOIS AT URBANA-CHAMPAIGN

THE GRADUATE COLLEGE

December 1994

WE HEREBY RECOMMEND THAT THE THESIS BY

GREGORY ALEXANDER KOSINOVSKY

ENTITLED THRESHOLD CURRENT AND MODULATION RESPONSE OF SEMICONDUCTOR LASERS

BE ACCEPTED IN PARTIAL FULFILLMENT OF THE REQUIREMENTS FOR THE DEGREE OF DOCTOR OF PHILOSOPHY

Director of Thesis Research

for Head of Department

Committee on Final Examination†

Chairperson

† Required for doctor's degree but not for master's.

O 517

THRESHOLD CURRENT AND MODULATION RESPONSE OF SEMICONDUCTOR LASERS

Gregory Alexander Kosinovsky, Ph.D.
Department of Electrical and Computer Engineering
University of Illinois at Urbana-Champaign, 1995
Karl Hess, Advisor

The possibility of carrier charge imbalance in the active region of quantum well lasers is demonstrated (in contrast to the usual presumption of charge neutrality in the region), and the resulting effect on the threshold current is examined. The investigations are performed with a simple rate equation simulator, as well as with a self-consistent laser simulator MINILASE. The models predict similar qualitative trends in threshold current dependencies.

A novel model is developed for the lasing threshold analysis of Vertical Cavity Surface Emitting Lasers based on the first principles analysis of resonant cavity E-M field enhancement by L.F. Register. The validity of the model is confirmed by comparison with the standard Fabry-Perot model for conventional edge emitting lasers. The utility of the new model in special cases of the Vertical Cavity Laser analysis is discussed.

A theoretical investigation of the effect of longitudinal-optic phonon imbalance on the modulation response of semiconductor lasers was performed using the MINILASE simulator. A novel formalism is developed for the inclusion of phonon-assisted capture into the self-consistent simulation. As a result, a new perspective on the role of hot phonons, which hitherto was thought to be strictly detrimental to the high frequency modulation response, was developed. Our simulations show that, depending on the value

of the carrier capture coefficient, nonequilibrium phonons may either improve or worsen the modulation bandwidth.

DEDICATION

To my wife Irina

ACKNOWLEDGEMENTS

The author would like to thank his thesis advisor, Professor Karl Hess, for his encouragement, guidance, and patience. His vast scientific knowledge has been an invaluable resource. Special thanks are due to author's collaborators, Mr. R. Baca, Prof. Z.S. Gribnikov, Dr. M. Grupen, Dr. L.F. Register, and Dr. G.H. Song. The author is also very thankful for the opportunity to work among and share ideas with so many talented researchers. Discussions with them were both a source of knowledge and much needed inspiration. Among the people the author would like to thank are Dr. J.D. Bude, Prof. S.-L. Chuang, Dr. Yu. Lyanda-Geller, Dr. J. Higman, Dr. C.H. Lee, Dr. V.B. Pevzner, Prof. U. Ravaioli, Dr. L. Rota, Dr. S. Seki, Dr. P. von Allmen, Dr. J. Wang, and Dr. P.D. Yoder.

TABLE OF CONTENTS

LIST OF TABLES

LIST OF FIGURES

CHAPTER 1

INTRODUCTION

Threshold current and modulation response are two of the most crucial characteristics of semiconductor lasers. As outlined in the classic texts [1, 2], the threshold current in lasers is the lowest bias current that allows the optical gain in one of the states of the system to reach a value equal to the sum of all optical losses. Since the gain and the optical losses are all nonexplicit system-dependent functions of bias current, the problem of the minimization of threshold current involves the maximization of optical gain and/or minimization of optical loss. The most straightforward way to minimize the distributed loss is to increase the mirror reflectivity. This, however, presents a problem in the cost of the process (growing reflective coating on a cleaved transverse edge of a crystal wafer), as well as in the available optical output (the more light that is reflected back, the less is transmitted out). Therefore, the most basic approach was to optimize the gain. An early important contribution towards that end was the *separate light confinement* [3], which allowed a high resonant optical field to be maintained in the ever shrinking *active region* – the region of the device where most electron-hole recombination takes place. The shrinkage of this region was prompted by the desire to decrease the number of electrons excited or "pumped" by the bias current, thus allowing for the decrease of the latter.

The drive for more efficient pumping also turned to reducing the density of lower lying carrier states, thus minimizing the wastful pumping of states not involved in lasing. This led to the research into lasers with lower dimensional carrier gas active regions – beyond the two-dimensional (quantum wells, or QW [4, 5]), to one-dimensional (quantum wires), and zero-dimensional (quantum dots)[6]–[8]. The research into quantum wires and dots is still highly experimental, and is hampered by complicated technological processes and the inability to reduce excessive optical losses.

One of the key impediments to efficient pumping is the large asymmetry in the dispersion relations of the conduction and valence bands of most lattice-matched III-V semiconductors, which leads to very uneven densities of states, and, consequently, pumping efficiency of the conduction and valence bands. This problem was highlighted in the paper by Yablonovich and Kane [9], who proposed that the best way of circumventing it was the use of *strained layer* quantum well laser technology [10], which allows for the reduction of the valence band effective mass [11].

Our proposal in Chapter 2 addresses the possibility of exploiting the band structure disparity of unstrained semiconductor lasers such as GaAs/AlGaAs to reduce the threshold current by effective modulation doping.

Chapter 3 deals with the threshold current analysis of an entirely different class of lasers – the Vertical Cavity Surface Emitting Lasers (VCSELs). These lasers present a relatively new development in technology [12]. These structures, as the name suggests, have their optical cavities oriented transversely to the plain of the interface, i.e., along the growth direction. This fundamentally planar technology holds great promise for

easier growth and interfacing, as well as 2-D laser array fabrication. It also, however, presents many challenges, not the least of these is the minuteness of the laser cavity, which greatly magnifies the distributed mirror loss and requires the mirror reflectivities to be above 0.99. The completely new features of VCSELs require a reevaluation of the entire approach in the basic threshold current analysis. The development and validation of such an approach are the bases of Chapter 3.

Finally, Chapter 4 deals with the problem of the high frequency laser modulation response. As the detailed review by Lau [13] indicates, the location of the resonant peak in the modulation response is primarily determined by the rate of interband recombination. However, as our earlier work demonstrates [14], the rates of intraband carrier transfers, such as those between the quantum well and three-dimensional regions greatly influence the shape of the modulation response characteristic. The carrier capture process has long been a subject of investigations, using both classical [15, 16] and quantum mechanical [17] – [20] approaches. Concurrently, many different groups reported direct experimental evidence of nonequilibrium longitudinal-optic (LO) phonons resulting from intraband relaxation of the excited carriers and the subsequent effect on phonon-carrier dynamics [21]–[29]. Consequently, researchers began to consider the effect of nonequilibrium (hot) phonons on carrier dynamics and the high speed performance of semiconductor QW lasers [30, 31]. A particularly direct approach to this problem was taken by Tsai et al. [31], in which a system of macroscopic rate equations, including that for the nonequilibrium longitudinal-optic (LO) phonon occupation number, was solved. The authors of this work reported finding a definitive "bottleneck effect" of the hot LO phonons on the laser

modulation response. We set out to solve a similar problem, but with the use of a self-consistent microscopic laser simulator MINILASE, which will be described in more detail in Chapter 2.

CHAPTER 2

EFFECT OF CARRIER CHARGE IMBALANCE ON THE THRESHOLD CURRENT IN DIODE LASERS

Macroscopic 1-D studies of threshold currents in QW lasers, based on the gain threshold condition and radiative rate equations, have frequently been done [32]–[35]. With increasing computer power, efforts have also been made to formulate self-consistent 2-D simulators for diode lasers [36]–[38]. These simulators are more precise for studying semiconductor lasers and, on occasion, necessary to quantitatively describe the combined physics of the carrier transport and the optical field. Here we describe a particular aspect of the physics of threshold current in ideal lasers.

In macroscopic 1-D investigations of the threshold current dependences [33]–[35], the balance of mobile charge (n=p), i.e., local charge neutrality, has been used as one of the constraints in the quantum well regions of PIN diodes. This is an accurate assumption for any sizable active region, since in normal device operation, Poisson's equation does not permit a large buildup of net charge. However, for the dimensions of quantum wells, this constraint loses its strict validity, since local charge neutrality is not necessarily preserved. It is difficult to see how such a charge imbalance can be incorporated without ad hoc assumptions into rate-equation-based simulators. We show here that the deviation from charge neutrality follows naturally in the solution of our self-consistent

simulator MINILASE, developed by Song, Grupen, and Hess [37, 39] (with 2-D Helmholtz eigenvalue solver developed by Kosinovsky [40]). We also show that this has important consequences for laser threshold currents.

2.1 Theoretical Investigations of Carrier Charge Imbalance Based on Rate Equations Model

Here we show the effect on the predicted threshold current that is obtained from a simple rate equation simulator when the n/p ratio, which is ordinarily assumed equal to 1, is varied. We ran a simulation based on solving the laser gain equation and used the fact that spontaneous emission dominates the diode laser current value at the onset of stimulated emission [33]–[35]. The following system of equations was solved:

$$r_{th}^{st} = \sum_i B(E_c^{\nu_0,i}, E_v^{\nu_0,i}) \cdot g(E_c^{\nu_0,i} - E_v^{\nu_0,i}) \cdot (f_e(F_c^{th}, E_c^{\nu_0,i}) + f_h(F_v^{th}, E_v^{\nu_0,i}) - 1) \qquad (2.1)$$

$$n(F_c^{th}) = k \times p(F_v^{th}) \qquad (2.2)$$

Here B is the Einstein coefficient, g is the reduced density of states (assuming no line broadening), f_e, f_h are the Fermi functions for electrons and holes respectively, and $E_c^{\nu_0,i}$, $E_v^{\nu_0,i}$ are the conduction and valence band levels (with respect to minimum of the i-th subband) contributing to lasing mode ν_0; F_c^{th}, F_v^{th} are the electron and hole Fermi levels at threshold; n and p are electron and hole concentrations in the well, respectively. The multiplicative factor k denoting the ratio between electrons and holes in the quantum well is explicitly set to 1 in most rate equation models. The stimulated emission at threshold

r_{th}^{st} is related to the total loss α by

$$\alpha \cdot v = \Gamma \cdot r_{th}^{st} \tag{2.3}$$

Here v is velocity of light in the medium and Γ is the optical confinement factor.

Equations (2.1) and (2.2) are solved for F_c^{th} and F_v^{th}, and the latter are used to calculate the total spontaneous emission rate at threshold $R_{sp,th}$. Assuming that most of the radiative current at threshold comes from spontaneous emission, we then have for nominal threshold current density:

$$J_{th} = R_{sp,th} \cdot e \cdot L \tag{2.4}$$

where e is the elementary charge and L is the QW width.

In the investigation, we used a particular structure with the quantum well width of 50 $\mathring{A}$, and the distributed loss factor of 5200m^{-1}, which was determined to be the total of distributed mirror loss, waveguide loss, and free carrier absorption loss for the structures investigated using the MINILASE simulation (to be described in more detail). By varying the k factor in 0.1 increments, we obtained the relation between this ratio and the laser threshold current shown on Fig. 2.1. We see that for this QW structure, a monotonic rise in the nominal threshold current density is predicted with the increase in the n/p ratio.

The reason for the variation of threshold current with the k=n/p ratio follows logically from the underlying physical model. Consider the Eq. (2.1) for the rate of stimulated

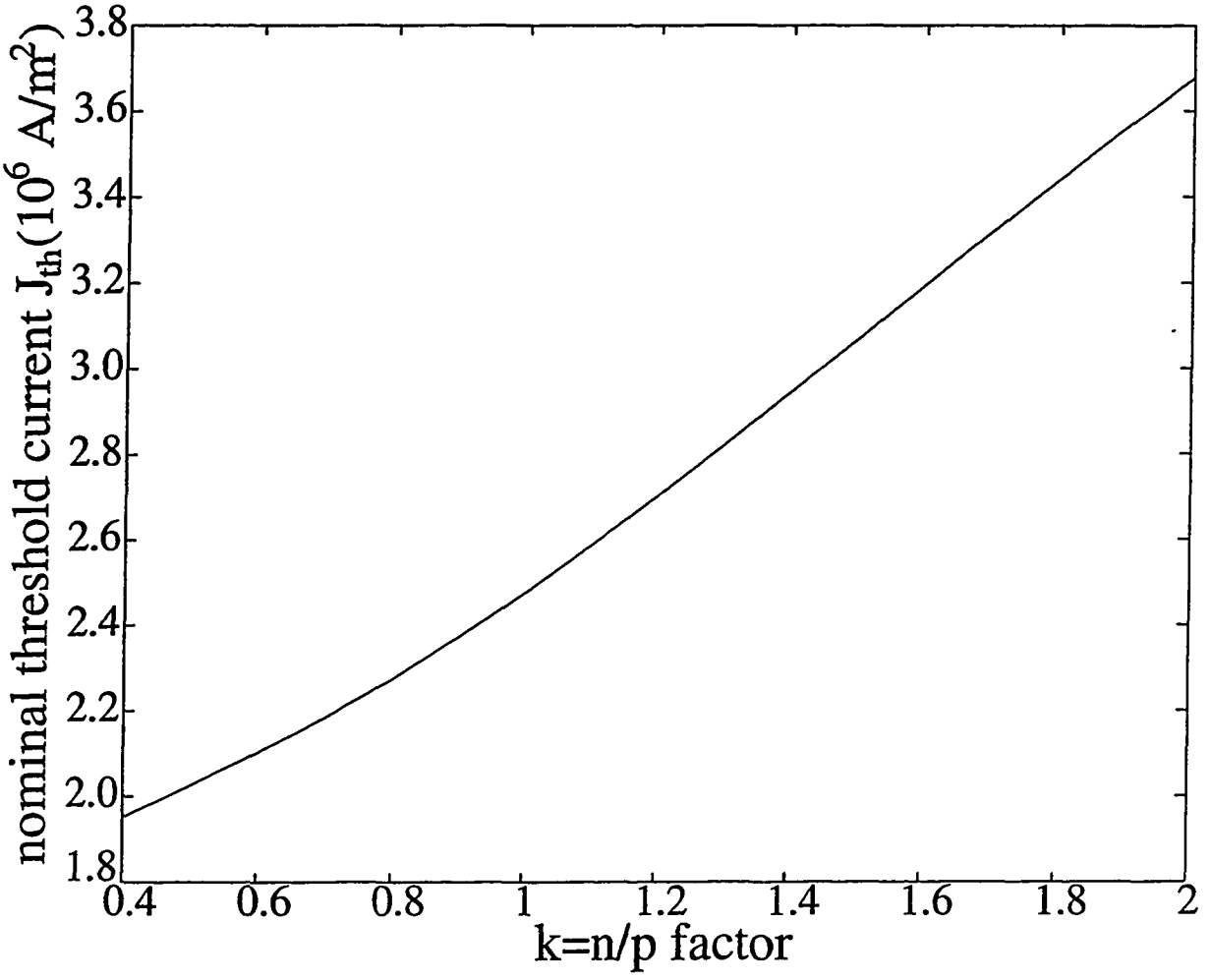

Figure 2.1 Nominal current density at threshold vs. k=n/p factor for the 1-D model.

emission (r_{th}^{st}) at threshold. Our calculations for a 50 $\AA$ well show that (for the given range of k) ν_0 is always the lowest allowable optical mode. Therefore, g is constant and has nonzero value only for i=1, B is constant, and f_e, f_h are functions of F_c^{th} and F_v^{th} only. Hence Eq. (2.1) reduces to the following:

$$r_{th}^{st} = A \cdot (f_e(F_c^{th}) + f_h(F_v^{th}) - 1) \tag{2.5}$$

where A is a known factor. Since r_{th}^{st} is fully determined by the gain threshold value $G_{th} = 5200m^{-1}$ (see discussion above), $f_e(F_c^{th})$ and $f_h(F_v^{th})$ must vary by equal and opposite amounts as k varies. Because of the effective mass disparity in GaAs (and most other materials), the slope of $f_e(F_c)$ at F_c^{th} is usually small, while the slope of $f_h(F_v)$ at F_v^{th} is large. For example, $\frac{\partial f_h}{\partial F_v^{th}} \approx 3.7 \cdot \frac{\partial f_e}{\partial F_c^{th}}$ for k=.6, and $\frac{\partial f_h}{\partial F_v^{th}} \approx 44 \cdot \frac{\partial f_e}{\partial F_c^{th}}$ for k=1.5. Therefore, as k=n/p increases, the increase in F_c^{th} is much greater than the decrease in F_v^{th}. Since the calculation of the threshold current involves the summation of terms including $f_e(F_c^{th}, E_c^{\nu,i}) \times f_h(F_v^{th}, E_v^{\nu,i})$ over all optical modes ν and subbands i (see Hess et al. [32]), it is clear that the large increase in F_c^{th} outweighs the much smaller decrease in F_v^{th}, and the threshold current will increase with k.

2.2 Application of the Self-Consistent Simulation

In order to determine whether the n-p imbalance and its consequences on threshold current are physically meaningful, we have employed the self-consistent 2-D simulator MINILASE, originally described in a previous paper [37]. It consists primarily of the

coupled discretized solution of Poisson's equation and the electron and hole current continuity equations:

$$-\nabla \cdot \epsilon \nabla \psi + q(n - p - N_D^+ + N_A^-) = 0 \tag{2.6}$$

$$\frac{dn}{dt} + \nabla \cdot j_e + U^{st}rad + U_{rad}^{sp} + U_{HSR} + U_{Aug} = 0 \tag{2.7}$$

$$\frac{dp}{dt} + \nabla \cdot j_h + U^{st}rad + U_{rad}^{sp} + U_{HSR} + U_{Aug} = 0 \tag{2.8}$$

Here ϵ is the permittivity of the material, ψ is the electrostatic potential, N_D^+,N_A^- are the concentrations of ionized donors and acceptors respectively, j_e,j_h are the particle currents of electrons and holes respectively, and U_{rad}^{st},U_{rad}^{sp}, U_{HSR},U_{Aug} are the electron and hole loss rates due to stimulated emission, spontaneous emission, Hall-Shockley-Reed recombination, and Auger recombination, respectively.

The above system is solved by the Newton iteration on its Jacobian. The solution variables of this system are the electrostatic potential and the electron and hole quasi-Fermi levels. In this formalism, the electron and hole quasi-Fermi levels are only loosely coupled. They are each primarily determined by their respective continuity equations. This point is crucial, because it allows the local charge imbalance that we report here. Note that the actual physical charge neutrality constraint is globally enforced through Poisson's equation. The n=p constraint that directly linked the electron and hole quasi-Fermi levels in most of the previous studies is not rigorously required by any physical law. Since the date of the aforementioned publication [37], one of the key changes has been [39] the addition of the Schroedinger Equation for the QW active region, solved

iteratively with the continuity-Poisson Newton system:

$$H\phi_i = E_i\phi_i \tag{2.9}$$

Here H is the Hamiltonian, and ϕ_i, E_i are the envelope wavefunctions and energy levels of the respective carrier subbands.

Considering the true quantum nature of the active region, this addition was critical in being able to investigate any physical effects related to the electronic properties of the active region, notably in our case, the charge distribution and the radiative recombination. More details on the quantum model of the well region and its coupling to the classical transport model in the 3-D regions of the device are given in a more recent publication [14], as well as in Chapter 4.

The electronic system is then solve iteratively with the photon rate equations:

$$\frac{dS_\nu}{dt} = G_\nu S_\nu + R_\nu^{sp} - \frac{S_\nu}{\tau_\nu} \tag{2.10}$$

Here S_ν is the photon mode population, G_ν is the gain, R_ν^{sp} is the spontaneous emission into the mode, and τ_ν is the photon lifetime. The mode index ν is over the range of possible lasing modes.

The 2-D Helmholtz eigenvalue equation is also solved to obtain the transverse optical field profile [40].

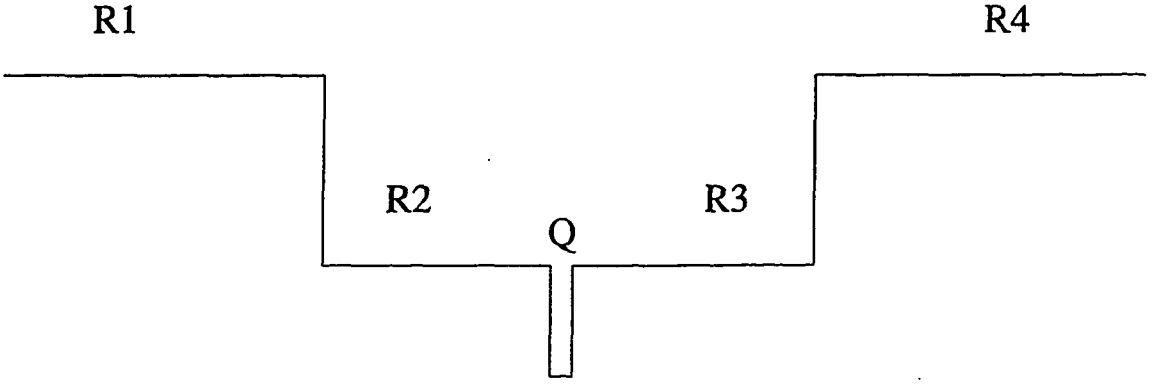

Figure 2.2 Idealized conduction band diagram of the laser cross-section. Doping concentrations corresponding to the labeled regions are given in the text.

2.2.1 Setup of the simulation experiment

The structure considered for our example is the quasi-one dimensional buried Separate Confinement Heterostructure (SCH) laser. Figure 2.2 illustrates the idealized conduction band structure cross-section of this device.

The doping profiles were varied in order to achieve the n-p imbalance and to investigate the resulting effects. The device has a total width of 3 μm and symmetric material structure. There is a 50$\AA$ $GaAs$ QW active region **Q** in the middle, then 975$\AA$ $Al_{0.4}Ga_{0.6}As$ light guiding regions **R2, R3** to each side, followed by 1.4μm $Al_{0.65}Ga_{0.35}As$ regions **R1, R4** bounded by electrodes.

We investigated three structures, which had different dopings in the regions **R1**, **R2**, **R3**, and **R4** on Fig. 2.2. In structure A, **R1** was p-doped at $5.0\times10^{18}cm^{-3}$, **R4** was n-doped at $5.0\times10^{18}cm^{-3}$, and the rest of the device was undoped. In structure B, **R1** and **R2** were p-doped at $3.0\times10^{18}cm^{-3}$, **R4** was n-doped at $2.0\times10^{18}cm^{-3}$, and the rest was undoped. Finally, in structure C, **R1** was p-doped at $3.0\times10^{18}cm^{-3}$, **R3** and **R4** were n-doped at $3.0\times10^{18}cm^{-3}$, and other regions were undoped. The doping concentrations were chosen not only to optimize the n-p imbalance in structures B and C, but also to achieve approximate equality of the gain threshold (loss factor) among the three structures.

2.3 Results and Discussion

Table 2.1 shows the results of the simulation. The first important result is that the n=p condition, often used as a constraint, is strongly violated in the asymmetrically doped structures (giving values of k=0.66 and k=1.47 for B and C structures, respectively). It is reassuring that the threshold current versus k=n/p ratio dependence for these structures follows qualitatively the trend suggested by the simplified calculation that led to Fig. 2.1. Quantitatively, there is about a 25% difference between the threshold current values obtained from MINILASE and listed in Table 2.1 and the corresponding points of Fig. 2.1. This difference is acceptable, considering the simplicity of the rate equation model and, in fact, underscores the importance of the self-consistent simulators for accurate quantitative analysis.

Table 2.1 Summary of simulation results for structures A, B, and C.

Structure	k=n/p	$J_{th}(A/m^2)$
A	1.05	3.38×10^6
B	0.66	2.78×10^6
C	1.47	4.16×10^6

Comparing the MINILASE data of Table 2.1 for different structures, we note that the lasing threshold current difference between structure B (k=0.66) and structure C (k=1.47) is a very considerable 49.4%. More important than the difference between the two asymmetrically doped structures, however, is the difference between structure A, representing a "conventional" PIN laser with n-p neutrality preserved, and structure B, where the heavy p-doping up to the quantum well results in a much higher concentration of holes than electrons in the well. We can see that decreasing the n/p ratio from 1 to 0.66 results in a 15.6% lowering of the threshold current value, which is a significant improvement.

2.4 Conclusion

It is important to emphasize, that the threshold current dependence on the n/p ratio is *entirely* due to the difference between the effective masses of electrons and holes. In a model simulation where the masses are equalized, the threshold current is *completely independent* of the carrier concentration ratio.

Finally, let us note that if the idea presented here for lowering threshold current is approached experimentally, better methods of modulation doping may be found. In particular, instead of heavy doping of the entire waveguide region on the p side (which raises the free carrier absorption, and thus the lasing threshold), δ-doping may be used, i.e. a thin heavily doped layer may be implanted near the quantum well. We did not take this approach in our simulation, because it would have required major changes in the

simulator, whereas the present approach was sufficient in demonstrating the postulated effect.

CHAPTER 3

NEW MODEL FOR CURRENT THRESHOLD ANALYSIS OF THE VERTICAL CAVITY SURFACE EMITTING LASERS

3.1 Introduction and Background

In recent years there have been a number of investigations of Vertical Cavity Surface Emitting Lasers (VCSELs), both experimental [12. 41] and theoretical [42]–[46]. In theoretical studies of VCSELs, some of the authors [45, 46] employed the traditional Fabry-Perot model for laser cavities, while others considered the microcavity effects on both the spontaneous emission [43, 44] and gain [42]. In the traditional theory, radiation is first modeled via the emission (and absorption) of photons into the "quasimodes" of the laser cavity. Subsequent radiation from the cavity is then modeled, typically via a lifetime term, as leakage from the quasimodes of the cavity to external "free-space" modes through partially transmitting boundaries. However, the questions raised by the latter group of authors [42]–[44] suggest a new approach may be required to model VCSELs.

3.2 New Model for Laser Threshold

To study lasing in general resonant cavities including both conventional and VCSEL structures, L.F. Register considered radiation directly into the electromagnetic modes of the *coupled* resonant-cavity–free-space system. Using this approach, a general expression for the steady-state photon emission into such a system was derived (see Register et al. [47]).

$$S \propto \left[\left(\frac{2}{\pi\hbar}\right) - G_{net,dis}\right]^{-1} \tag{3.1}$$

Here S is the rate of photon emission. $G_{net,dis}$ is the *distributed* net gain (per unit energy) inside the resonant cavity, and contains the effects of optical field resonances/antiresonances within the cavity both as a function of frequency and position. These resonance effects are calculated by Register and R. Baca via both eigenstate calculations and a Green's function approach for Maxwell's equations. The pole in the photon emission rate as distributed gain approaches the value $\frac{2}{\pi\hbar}$ is suggestive, since, in the steady-state lasing regime, the ideal photon emission rate may grow indefinitely with increase in current bias, while gain remains constant.

To establish the relationship between Eq. (3.1) and the conventional threshold analysis, G.A. Kosinovsky and L.F. Register applied the conventional lasing threshold analysis to the large cavity of length L in Fig. 3.1.

$$G_{net,md} = \frac{1}{\tau} \tag{3.2}$$

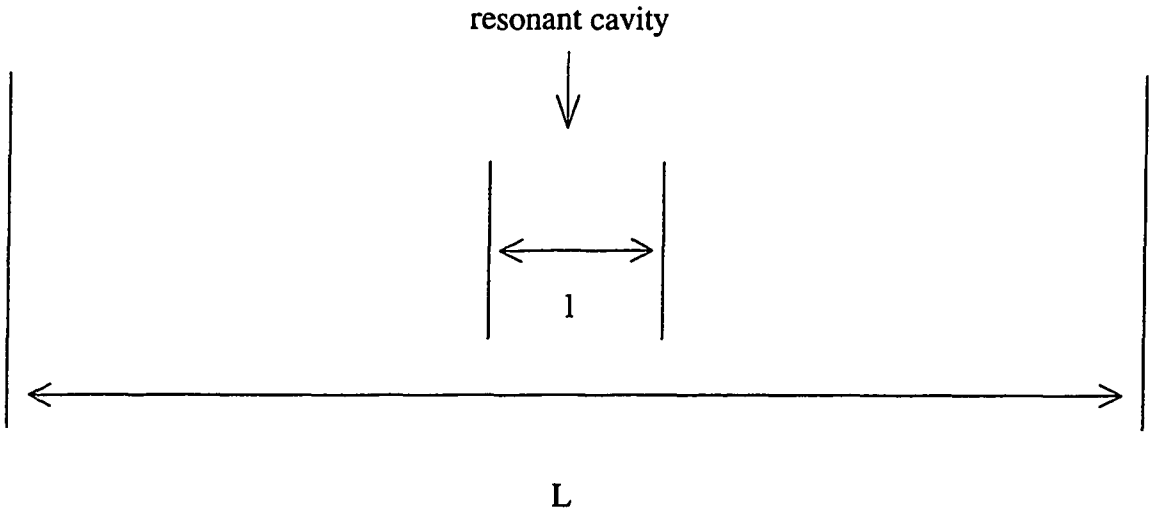

Figure 3.1 A schematic diagram of "outer cavity" region of free space of length L with a small resonant cavity of length l in the middle.

Here $G_{net,md}$ is the net gain per mode, and τ is the cavity photon lifetime of the given mode. Clearly, $G_{net,md}$ is the integral of $G_{net,dis}$ over the mode width $\Delta\hbar\omega$, where $\Delta\hbar\omega$ is the period of the resonant spectrum for a cavity of length L. Figure 3.2 illustrates the relationship between the distributed gain formalism, shown by the continuous spectrum and the small cavity net gain formalism, shown by the discrete spectrum. Necessarily, the periods of both spectra have the same period $\Delta\hbar\omega$ determined by the inner cavity l of Fig. 3.1.

Since the "end mirrors" of the large cavity are fully transmitting, the large cavity lifetime of a photon originating inside the small resonant cavity is $\tau = \tau_0 + \tau_1$, where τ_0 is the photon lifetime of the resonant cavity, and $\tau_1 = \frac{L-l}{2c}\left|\frac{k}{k_z}\right|_{fs}$ is the time it takes for a photon to travel from just outside the resonant cavity to the edge of the large cavity. Here, c is the free-space velocity of light, and $\left|\frac{k}{k_z}\right|_{fs}$ is the ratio of the photon wavevector

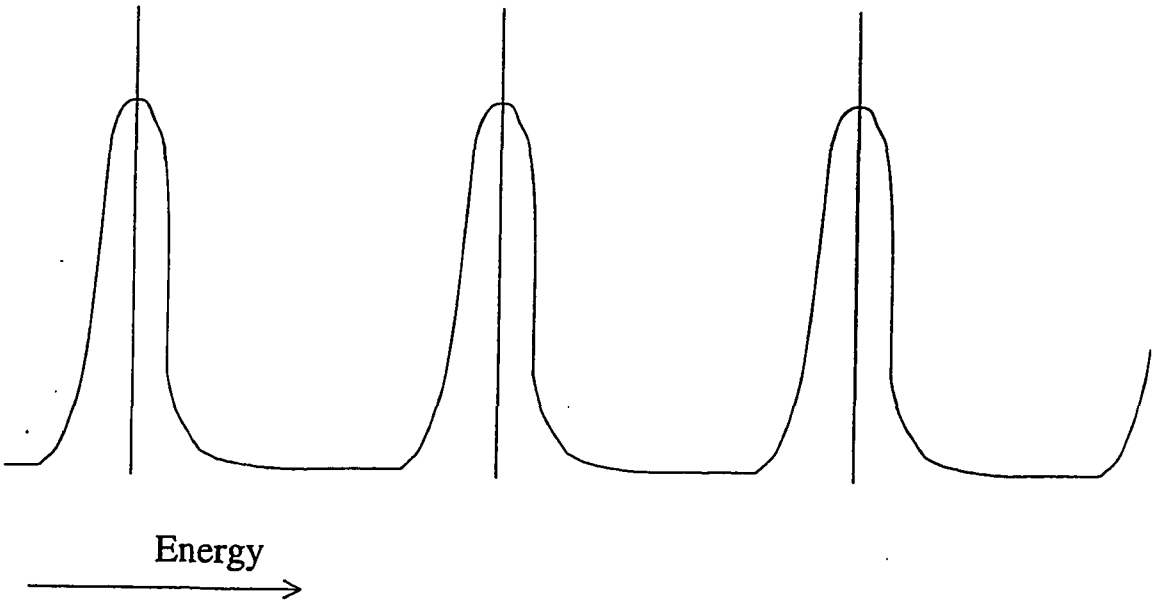

Figure 3.2 A schematic diagram of the continuous (distributed) and discrete (modal) gain spectra.

to its component in the resonant direction in free space. Thus we have

$$\int_{\Delta\hbar\omega} G_{net,dis} = \frac{1}{\tau_0 + \tau_1} \tag{3.3}$$

Now let's examine the above equation in two extreme limits of L. As L becomes very large compared to l, $\tau \rightarrow \frac{L}{2c}\left|\frac{k}{k_z}\right|_{fs}$ and $\delta\hbar\omega = \frac{\pi\hbar c}{L}\left|\frac{k_z}{k}\right|_{fs}$ becomes so small that only a single value of the integrand in Eq. (3.3) is selected. Since the mode with the most gain is the one that defines threshold, Eq. (3.3) becomes

$$G^{max}_{net,dis} = \frac{1}{\tau\Delta\hbar\omega} = \frac{2}{\pi\hbar} \tag{3.4}$$

so we can see explicitly how the value $\frac{2}{\pi\hbar}$ defines threshold.

If we take the other extreme limit $L \to l$, then $\tau \to \tau_0$, and Eq. (3.3) goes to

$$\int_{\delta\hbar\omega} G_{net,dis} = \frac{1}{\tau_0} \tag{3.5}$$

Here

$$\delta\hbar\omega = \frac{\pi\hbar c}{nl}\left|\frac{k_z}{k}\right|_{mate} \tag{3.6}$$

is the resonance period of the laser structure of length l in the z-direction. Here subscript *mate* refers to the material the laser is made of, and n is the refractive index of this material. Thus $\int_{\delta\hbar\omega} G_{net,dis}$ is the conventional modal gain of a laser structure and Eq. (3.5) is the conventional laser threshold equation. Since Eqs. (3.4) and (3.5) are just different limiting cases of Eq. (3.3), we expect Eq. (3.4) to give the same result for conventional laser structures as the conventional theory (Eq. (3.5)), which the computational results to be presented will confirm. For VCSELs, the relationship between the results of Eqs. (3.4) and (3.5) is not so clear, mainly because the definition of the photon mode lifetime t_0 of a VCSE cavity is ambiguous. For a conventional Fabry-Perot cavity with length l and mirror reflectivities R_1, R_2,

$$\tau_0 = \frac{nl}{2c\left|\frac{k_z}{k}\right|_{mate}}\left[1 + \frac{(R_1 + R_2 + 2R_1R_2)}{1 - R_1R_2}\right] \tag{3.7}$$

However, consider the typical VCSEL structure shown in Fig. 3.3. One can see that the "waveguide" region is as small as 1 wavelength of light, whereas the mirrors are many

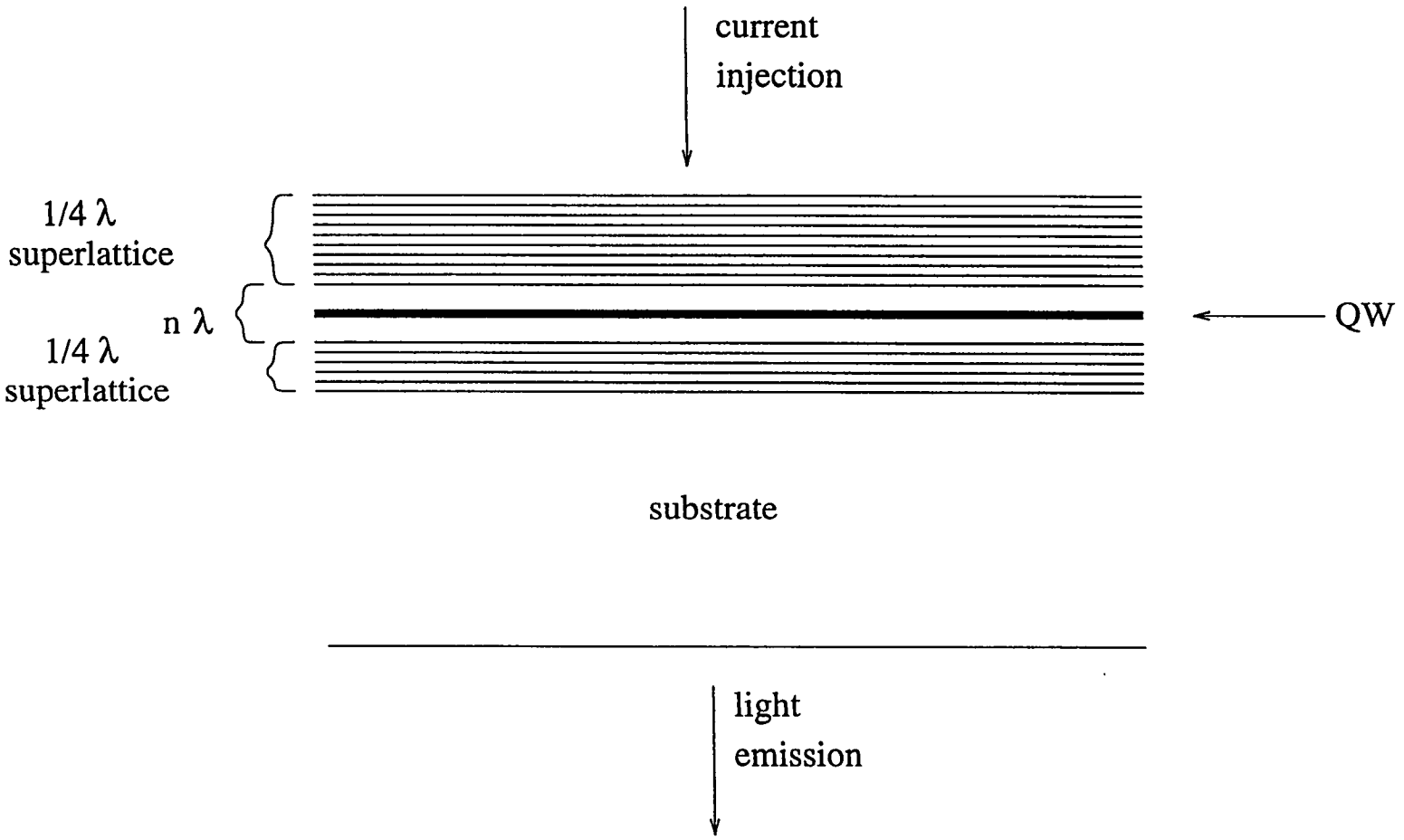

Figure 3.3 Typical VCSEL structure.

wavelengths thick. Hence, what is the length l of a VCSE structure? Does it include any of the Bragg reflector mirror layers? More generally, does it make sense to talk about a Fabry-Perot cavity one wavelength long? These are clearly some of the questions to be addressed. Note that Eq. (3.4) does not contain any ambiguous quantities for either VCSE or conventional structure analysis.

3.3 Adaptation of the Conventional Threshold Gain Equation to the Distributed Gain Formalism

We now consider the gain $G^{lc}_{net,md}$ of a single longitudinal mode of a large cavity of length L (which has a small resonant gain cavity of length l in the middle). Using the conventional discrete single-mode gain approach (and ignoring losses other than stimulated emission for now), we would have, if the gain medium were invariant in the z-direction,

$$G^{lc}_{net,md} = \int d^3r B g_{red}(f_c - f_v)|\phi_{xy}|^2_{norm}\frac{1}{L} \tag{3.8}$$

Here g_{red} is the reduced density of states of electrons and holes for interband transition, f_c, f_v are the Fermi occupation probabilities for electrons and holes, $|\phi_{xy}|^2_{norm}$ is the square of the transverse electric field profile of the optical mode, normalized to unity, and B is the Einstein B-coefficient for the gain medium,

$$B = \frac{1}{n^2}B_{fs} \tag{3.9}$$

Here B_{fs} is the free-space value of the Einstein B-coefficient.

If it is the case (as we certainly have here) that the electrical field profile undergoes significant change along the z-direction inside the length L, then the B factor in Eq. (3.8) must be replaced with

$$B_{new} = B_{fs} * \frac{|\phi_z|^2_{norm}}{\overline{|\phi_z|^2_{norm}}} \tag{3.10}$$

Here $\overline{|\phi_z|^2_{norm}}$ is the average value of the square of the longitudinal electric field profile, and is equal to the free space value if L is large enough. Therefore, from Eqs. (3.8), (3.9), and (3.10)

$$G^{lc}_{net,md} = \frac{n^2}{L}\left[\int dxdyBg_{red}(f_c - f_v)|\phi_{xy}|^2_{norm}\right]\int_l dz \frac{|\phi_z|^2_{norm}}{\overline{|\phi_z|^2_{norm}}} \tag{3.11}$$

Here the quantity in brackets can be integrated separately under the assumption that it is constant inside the small resonant cavity and 0 outside. The fact that this quantity vanishes outside the resonant cavity is the reason for l being the region of integration over the z-direction. We also assumed that the longitudinal resonant electric field profile is not a function of transverse coordinates. Now, the bracketed quantity in the above equation is the single mode gain $G^{sc}_{net,md}$ of the small resonant cavity. Thus

$$G^{lc}_{net,md} = \frac{n^2}{L} G^{sc}_{net,md}\int_l dz \frac{|\phi_z|^2_{norm}}{\overline{|\phi_z|^2_{norm}}} \tag{3.12}$$

Taking the above expression for $G^{lc}_{net,md}$ and recalling that $\Delta\hbar\omega = \frac{\pi\hbar c}{L}\left|\frac{k_z}{k}\right|_{fs}$, we can finally write

$$G_{net,dis} = \frac{G^{lc}_{net,md}}{\Delta\hbar\omega} = \frac{n^2}{\pi\hbar c}\left|\frac{k}{k_z}\right|_{fs} G^{sc}_{net,md}\int_l dz \frac{|\phi_z|^2_{norm}}{\overline{|\phi_z|^2_{norm}}} \tag{3.13}$$

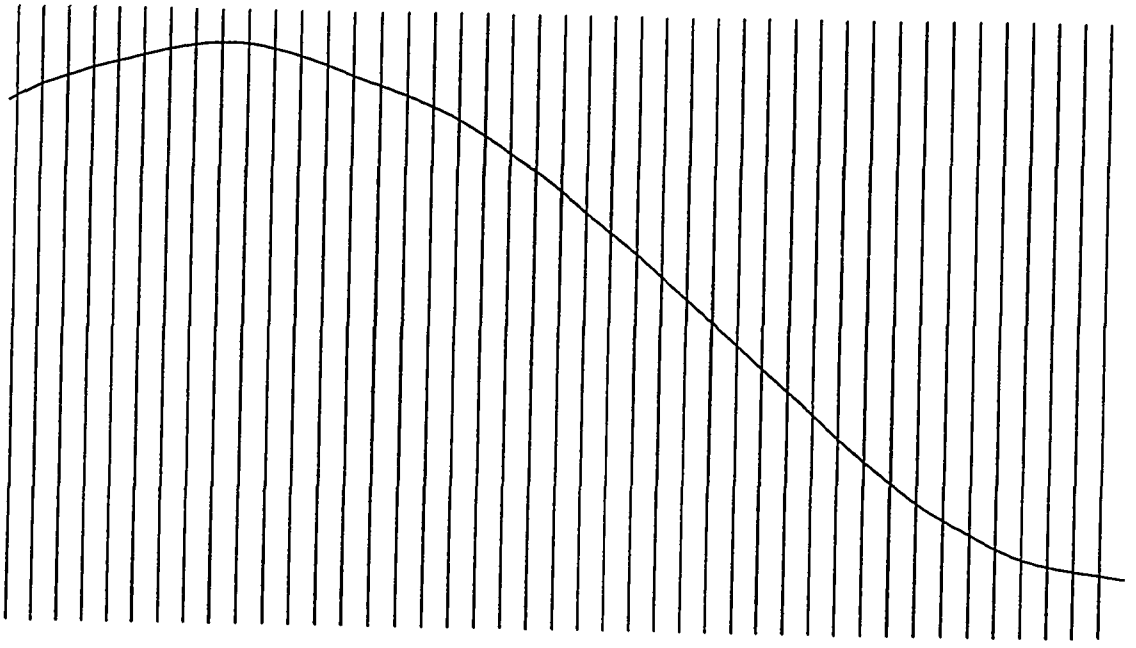

Figure 3.4 Superposition of a net large cavity spectrum on the distributed gain spectrum.

The justification for Eq. (3.13) is easy to see by examining Fig. 3.4, which superimposes the discrete spectrum of the *large* cavity of period $\Delta\hbar\omega$, determined by the arbitrarily large length L on the continuous distributed gain spectrum of period $\delta\hbar\omega$, determined by the resonant cavity length l. We can take L large enough to make sure that the continuous spectrum is nearly constant on the scale of $\Delta\hbar\omega$.

In deriving Eq. (3.5) we assumed that

$$G^{sc}_{net,md} = \int_{\delta\hbar\omega} G_{net,dis} \tag{3.14}$$

Thus, from Eqs. (3.13) and (3.14),

$$G^{sc}_{net,md} = G^{sc}_{net,md} \frac{n^2}{\pi\hbar c} \left|\frac{k}{k_z}\right|_{fs} \int_{\delta\hbar\omega} \int_{l} dz \frac{|\phi_z|^2_{norm}}{|\phi_z|^2_{norm}} \tag{3.15}$$

We can take the average of $\frac{|\phi_z|^2_{norm}}{|\phi_z|^2_{norm}}$ over l and $\delta\hbar\omega$ and rewrite the above as

$$G^{sc}_{net,md} = G^{sc}_{net,md}(l)(\delta\hbar\omega) \frac{n^2}{\pi\hbar c} \left|\frac{k}{k_z}\right|_{fs} \left(\frac{|\phi_z|^2_{norm}}{|\phi_z|^2_{norm}}\right)_{\text{avg. over } l,\ \delta\hbar\omega} \tag{3.16}$$

Finally, substituting Eq. (3.6) into Eq. (3.16), we obtain

$$\left(\frac{|\phi_z|^2_{norm}}{|\phi_z|^2_{norm}}\right)_{\text{avg. over } l,\ \delta\hbar\omega} = \frac{1}{n} \left|\frac{k_z}{k}\right|_{fs} \left|\frac{k}{k_z}\right|_{mate} \tag{3.17}$$

The above has to hold if the trivial relationship

$$G^{sc}_{net,md} = G^{sc}_{net,md} \tag{3.18}$$

is to hold. The numerical calculations performed by R. Baca for a resonant enhancement profile of a particular conventional diode laser structure agreed with Eq. (3.17) to four significant digits.

3.4 Verifying the Equivalence of Conventional and New Threshold Equations for Conventional Structures

The preceding section provided the analytical expression (Eq. (3.13)) for the distributed gain formalism. We can now use it to verify the equivalence of Eqs. (3.4) and (3.5) for conventional diode laser structures. From Eqs. (3.4) and (3.13) we obtain

$$G_{net,dis}^{max} = \frac{n^2}{\pi\hbar c}\left|\frac{k}{k_z}\right|_{fs} G_{net,md}^{sc}\int_l dz\left(\frac{|\phi_z|^2_{norm}}{\overline{|\phi_z|^2_{norm}}}\right)_{\text{max. over } \delta\hbar\omega} = \frac{2}{\pi\hbar} \tag{3.19}$$

Therefore,

$$G_{net,md}^{sc}\left(\frac{|\phi_z|^2_{norm}}{\overline{|\phi_z|^2_{norm}}}\right)_{\text{max. over } \delta\hbar\omega,\ \text{avg. over } l} = \frac{2c}{n^2 l}\left|\frac{k_z}{k}\right|_{fs} \tag{3.20}$$

We now have Eq. (3.16) derived from Eq. (3.5), and Eq. (3.20) derived from Eq. (3.4). We substitute Eq. (3.20) into Eq. (3.16), (using also Eqs. (3.5), (3.6) and (3.14)).

$$\frac{\left(\frac{|\phi_z|^2_{norm}}{|\phi_z|^2_{norm}}\right)_{\text{max. over } \delta\hbar\omega,\ \text{avg. over } l}}{\left(\frac{|\phi_z|^2_{norm}}{|\phi_z|^2_{norm}}\right)_{\text{avg. over } l,\ \delta\hbar\omega}} = \frac{\tau_0}{\frac{nl}{2c}\left|\frac{k}{k_z}\right|_{mate}} \tag{3.21}$$

If the above relation holds, then the threshold criteria of Eqs. (3.4) and (3.5) are equivalent for conventional diode lasers. Simulation results obtained by Baca showed Eq. (3.21) to hold to 4 significant digits.

3.5 Comparing the Results of Conventional and New Threshold Equations for VCSEL Structures

Let us now repeat the analysis of the previous section for VCSE lasers. As previously mentioned, there is an ambiguity in applying Eqs. (3.5) and (3.7) to the VCSE lasers because the definition of l is ambiguous. Assume, for now, that l is the length of the middle portion of the VCSE laser, excluding the quarter-wave Bragg superlattices (which make up the larger length of the device). Thus, l is a small integral number of wavelengths of light (usually 1). In that case, the only difference between VCSELs and conventional structures is that the active region is confined to a tiny region of l (we designate its location $z = 0$), whereas in conventional structures the active region spans the length l (or, in some variations, a large part of it), Thus we can apply the Eq. (3.21) to the present analysis, as long as we replace "averaging over l" by "evaluation at $z = 0$":

$$\frac{\left(\frac{|\phi_z|^2_{norm}}{|\phi_z|^2_{norm}}\right)_{\text{max. over } \delta\hbar\omega, \text{ at } z=0}}{\left(\frac{|\phi_z|^2_{norm}}{|\phi_z|^2_{norm}}\right)_{\text{avg. over } \delta\hbar\omega, \text{ at } z=0}} = \frac{\tau_0}{\frac{nl}{2c}\left|\frac{k}{k_z}\right|_{mate}} \tag{3.22}$$

In this case too, numerical analysis shows complete agreement of the two theories!

3.6 Discussion

What conclusions can we draw from the results of the previous section? One, it shows that applying conventional theory to VCSE lasers is numerically meaningful, as long as one defines the cavity length to exclude all of the superlattice. Is the usefulness of the new theory, then, confined to simply verifying the validity of the old one for VCSE structures?

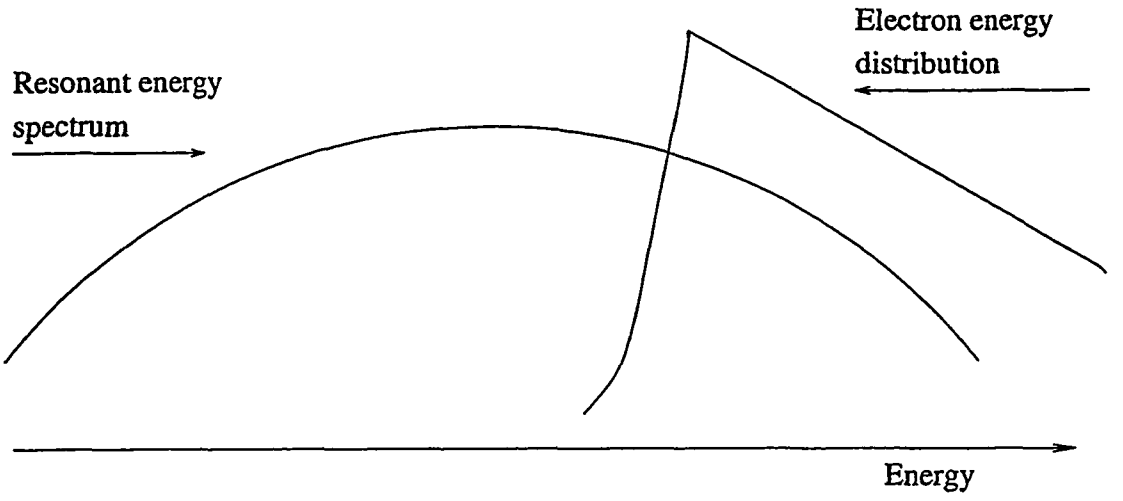

Figure 3.5 Superposition of the electron energy spectrum and the resonant gain spectrum, which peak at different energies.

The answer is no, if one looks at the previous analysis more closely. In writing Eq. (3.19) we assumed that the local peaks of the distributed gain and the resonant enhancement spectra occur at the same place. This, of course, is true if the resonant enhancement peaks are very narrow, as is the case for conventional diode lasers. Register and Baca's calculations show, however, that the resonant enhancement factor for a VCSE cavity retains about 90% of its peak value over a range of about 28 meV. This means that the peak of distributed gain may be determined by the peak of carrier energy distribution, and may occur at different energy than the resonant enhancement peak (see Fig. 3.5).

Since in the degenerate carrier concentration regime Fermi levels are very sensitive to small gain variations, a difference of several percent in gain calculations can result in significant difference in threshold current. Therefore, one should be able to account more accurately for the threshold current dependencies of the VCSE laser structures (as

well as for the exact lasing frequency calculations) by employing the distributed gain formalism (Eq. (3.4)) for the analysis and simulation. Register and Baca are currently implementing the distributed gain formalism into a 1-D version of the self-consistent laser simulator MINILASE, developed by R. Baca from the 2-D versions of Song et al. [37] and Grupen and Hess [39].

CHAPTER 4

HOT PHONON EFFECTS ON HIGH FREQUENCY MODULATION OF SEMICONDUCTOR LASERS

In Chapter 2 the numerical and physical approach to laser simulation in MINILASE was described. In the early version of the simulator, however, the carrier transport between the bulk waveguide region and the quantum well active region was accomplished via thermionic emission. While this model, which assumes instantaneous carrier capture and emission, is sufficient for steady-state calculations, it has serious deficiencies in transient simulation applications.

4.1 Simulating High Speed Performance

To simulate the high frequency modulation response correctly, a better model for carrier capture into the quantum wells has to be introduced, instead of the thermionic emission approach originally in place. The introduction of this model, which we summarize here, led to the first successful high-speed laser modulation analysis using a physical self-consistent simulator [14].

In the new approach, the carriers in the vicinity of the well were classified into two categories: the free particles and the bound particles. The two populations were assumed

to be in thermal equilibrium with themselves, but not with each other. Then the capture and emission rates R_{cap}, R_{em} can be represented as follows:

$$R_{cap} = \int_{E_c^0}^{\infty} dE_c \int_{E_w^0}^{E_c^0} dE_w M g_c g_w f_c (1 - f_w) \tag{4.1}$$

$$R_{em} = \int_{E_c^0}^{\infty} dE_c \int_{E_w^0}^{E_c^0} dE_w M g_c g_w (1 - f_c) f_w e^{E_w - E_c} \tag{4.2}$$

where subscripts c and w represent free and captured (conduction and well) particles respectively, E is energy, M is the transition matrix element, g is density of states, f is Fermi distribution function, and F is the Fermi energy. The $e^{E_w - E_c}$ factor approximates the cumulative Bose factor for the emission process. E_c^0 and E_w^0 refer to the top and bottom of the quantum well respectively. Figure 4.1 illustrates this process. Note that the energies are given in units of kT (Boltzmann factor times the temperature).

Given this model we can perform the following analytical manipulation:

$$\begin{aligned} f_w e^{E_w - E_c}(1 - f_c) &= \frac{1}{e^{E_w - F_w} + 1} e^{E_w - E_c} \left(1 - \frac{1}{e^{E_c - F_c} + 1}\right) \\ &= \frac{e^{E_w}}{e^{E_w - F_w} + 1} e^{-E_c} \frac{e^{E_c - F_c}}{e^{E_c - F_c} + 1} \\ &= e^{F_w} \frac{e^{E_w - Fw}}{e^{E_w - F_w} + 1} e^{-F_c} \frac{1}{e^{E_c - F_c} + 1} \\ &= e^{F_w - F_c}(1 - f_w) f_c \end{aligned} \tag{4.3}$$

Therefore, it follows from Eqs. (4.1) and (4.2) that

$$R_{em} = e^{F_w - F_c} R_{cap} \tag{4.4}$$

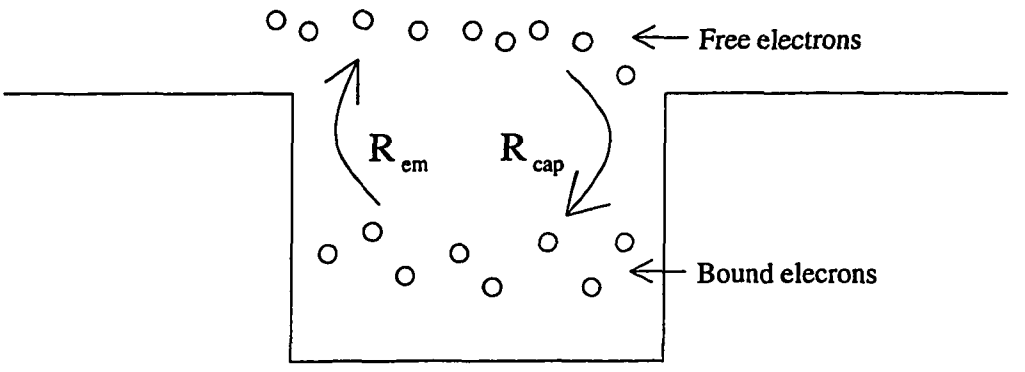

Figure 4.1 Diagram of the emission and capture processes of electrons into QW.

This resultant formula is physically consistent, since it predicts that in the case of complete thermal equilibrium between free and captured electrons (or holes), i.e., if $F_w = F_c$, the capture and emission rates are equal.

4.2 Model for Studying the Nonequilibrium Phonon Effects

The nonequilibrium phonon effects have been considered for a long time [21, 22]. In recent publications [30, 31], the effects of nonequilibrium phonon density on the modulation response of diode lasers had been investigated using the rate equation model and considering the effect of hot phonons on the nonlinear gain effects due to carrier heating. Here we propose a model for investigating in the self-consistent framework the effect

of phonon imbalance on the capture and emission rates of carriers in the well, and the subsequent effects on the modulation response.

We modify the capture/emission model described in the previous subsection using the common assumption [13] that the capture and emission processes are dominated by the LO phonon scattering. The inclusion of LO phonons leads to the following changes in the rates.

The Bose statistical factor used in Eq. (4.1) for R_{cap} is 1. A better approximation is to use the factor $(1+n_{ph})$, where n_{ph} is the Bose occupation number for the LO phonons, which, at equilibrium, has the value $n_{ph,eq} = \frac{1}{e^{\hbar\omega_{LO}}-1}$, where $\hbar\omega_{LO}$ is the energy of LO phonons relative to kT.

The Bose statistical factor used in Eq. (4.2) for R_{em} is $e^{E_w-E_c}$. We want to separate from it the part associated with the emission of high energy bound carriers into the free carrier population and to account for the nonequilibrium phonon effects. Thus the new Bose occupation number for emission is $e^{E_w-E_c+\hbar\omega_{LO}}n_{ph}$, where $e^{-\hbar\omega_{LO}}$ approximates the equilibrium phonon occupation number. The last approximation is necessary to assure the model's consistency when free and bound carriers are at or near mutual thermal equilibrium, as will be shown below.

Therefore, in place of Eqs. (4.1) and (4.2), we have

$$R_{cap} = \int_{E_c^0}^{\infty} dE_c \int_{E_w^0}^{E_c^0} dE_w M g_c g_w f_c (1-f_w)(1+n_{ph}) \tag{4.5}$$

$$R_{em} = \int_{E_c^0}^{\infty} dE_c \int_{E_w^0}^{E_c^0} dE_w M g_c g_w (1-f_c) f_w e^{E_w-E_c+\hbar\omega_{LO}} n_{ph} \tag{4.6}$$

Using Eqs. (4.5) and (4.6) instead of (4.1) and (4.2) in the analysis which led to Eqs. (4.3) and (4.4), we get the following result:

$$(1+n_{ph})R_{em} = e^{F_w - F_c + \hbar\omega_{LO}} n_{ph} R_{cap} \tag{4.7}$$

In the case of overall thermal equilibrium ($F_w = F_c$), the above equation assures that there is no unphysical net capture or emission ($R_{em} = R_{cap}$).

We now follow the formal derivation of the net capture rate $U_{cap} = R_{cap} - R_{em}$ given in a previously cited paper [14], but with inclusion of nonequilibrium phonons. Assuming that the matrix element M is constant (or averaged over the relevant energy range), we obtain (for electrons) from Eqs. (4.5), (4.6), and (4.7) the equality

$$U_{cap} = M\left[\left(\int_{E_w^0}^{E_c^0} g_w dE_w\right) n_{3D} - n_{2D} n_{3D}\right] \times \left[(1+n_{ph}) - n_{ph} e^{F_w - F_c + \hbar\omega_{LO}}\right] \tag{4.8}$$

where the concentration of bound electrons is $n_{2D} = \int_{E_w^0}^{E_c^0} g_w f_w dE_w$, and the concentration of free electrons is $n_{3D} = \int_{E_c^0}^{\infty} g_c f_c dE_c$. In the paper [14], the carrier capture coefficient $c_n = M \int_{E_w^0}^{E_c^0} g_w dE_w$ is defined and estimated from an earlier publication [16] to be in the range of $1 \times 10^{12} s^{-1}$ to $2 \times 10^{13} s^{-1}$. Given this definition, Eq. (4.8) becomes

$$U_{cap} = c_n \left(n_{3D} - \frac{n_{2D} n_{3D}}{\int_{E_w^0}^{E_c^0} g_w dE_w}\right) \times \left[(1+n_{ph}) - n_{ph} e^{F_w - F_c + \hbar\omega_{LO}}\right] \tag{4.9}$$

A similar expression follows for holes.

Now we have to define a relationship between U_{cap} and n_{ph}, which would allow a self-consistent solution for both the phonons and carriers. Let D_{ph} be the density of phonons in the active region. Then, in a small time step Δt, the change in LO phonon density due to carrier capture is $\Delta D_{ph} = U_{cap}\Delta t \times \alpha$ where α is the average number of LO phonons emitted in the complete downward transition from a free to a bound state (or the average number absorbed in the reverse process), and α is at least one and is on the order of unity. It may be different for the electron and hole capture processes, and the electron and hole contributions add to the total of ΔD_{ph}. We must consider also the loss of LO phonons to acoustic modes, which gives the final expression

$$\Delta D_{ph} = \left(U_{cap,el} \times \alpha_{el} + U_{cap,hl} \times \alpha_{hl} - \frac{D_{ph} - D_{ph,eq}}{\tau_{loss}} \right) \Delta t \tag{4.10}$$

Here $D_{ph,eq}$ is the equilibrium phonon density and τ_{loss} is the time constant associated with the LO phonon loss to acoustic modes (see Hess et al. [22]). We assign to τ_{loss} the early experimental value of $5 \times 10^{-12} s$, obtained from the literature [21]. A more recent experimental paper reports a nearly identical LO phonon lifetime value of 4 ps at 300 K [25].

To formally complete the self-consistent carrier-phonon problem, we now have only to relate D_{ph} and n_{ph}. Clearly, this is given by the relation

$$n_{ph} - n_{ph,eq} = \frac{D_{ph} - D_{ph,eq}}{g_{ph}} \tag{4.11}$$

Here g_{ph} is the density of states of LO phonons in the relevant range of k-space.

Hence, to calculate the nonequilibrium phonon occupation number, a good estimate of g_{ph} is needed. Using the Einstein model for optical phonons [48], we can write an energy-dependent phonon density of states function

$$g_{ph}^{E} = \int \frac{d^3q}{(2\pi)^3}\delta(E - \hbar\omega_{LO}) \tag{4.12}$$

Here q spans the First Brillouin Zone (FBZ). Since $\hbar\omega_{LO}$ does not have a strong q dependence, the delta function may be taken out of the integral, and we can treat it as a part of the energy conservation constraint separately from the function

$$g_{ph} = \int \frac{d^3q}{(2\pi)^3} \tag{4.13}$$

Now, the limits of integration in the expression above are much smaller than the actual FBZ boundaries $\frac{\pi}{a}$, where a is the lattice constant ($\approx 5.5\mathring{A}$ for GaAs). In practice, since the wavevector of electrons in the valleys is generally less than $0.1(\frac{\pi}{a})$, this is also the upper limit on the relevant q range (by conservation of momentum). This upper limit is confirmed by the plots of the phonon spectra presented in the previously cited papers [22, 26]. We can include the uncertainty of this range by taking it to be $\beta \times 0.1(\frac{\pi}{a})$, where β is close to and may be less than unity. Given these considerations, we obtain from Eq. (4.13) the following result:

$$g_{ph} = \beta \times 10^{24} m^{-3} \tag{4.14}$$

This completes the derivation of the model.

4.3 Simulation and Results

To study the effect of including the nonequilibrium phonon occupation, we ran the MINILASE simulations for a quasi-one-dimensional GaAs/AlGaAs laser structure with 100 $\AA$ GaAs quantum well. We varied the carrier capture coefficient in the range previously indicated. Three different values were used, and for simplicity of analysis, the electron and hole coefficients c_n and c_p were made to equal each other in all three cases, although this is generally not true. Also, the uncertainty factors α in Eq. (4.10) and β in Eq. (4.14) were assigned the value of one.

The values for (c_n, c_p) that were used were the extreme values of 2×10^{13} (Case A) and 1×10^{12} (case B), as well as an intermediate value of 4×10^{12} (case C). In each of the three cases, the time-dependent simulations were performed and modulation response curves obtained for two different models – one which kept the phonon occupation number fixed at its thermal equilibrium value, and one which allowed it to vary self-consistently with transient simulation according to the method described above.

The results obtained for the three cases are shown in Figs. 4.2 a), b), and c). We observe that in case B (lower estimate for capture coefficient) the results were as predicted by Tsai et al. [31]; however, in the opposite limit (case A) the reverse was observed – the inclusion of hot phonons actually *improved* the predicted modulation response. For the intermediate capture coefficient value (case C), the modulation curves are nearly equal.

For a closer look at the physics behind the results of Fig. 4.2, we look at the plot (Fig. 4.3) of the difference between the net capture rate with hot phonons included and

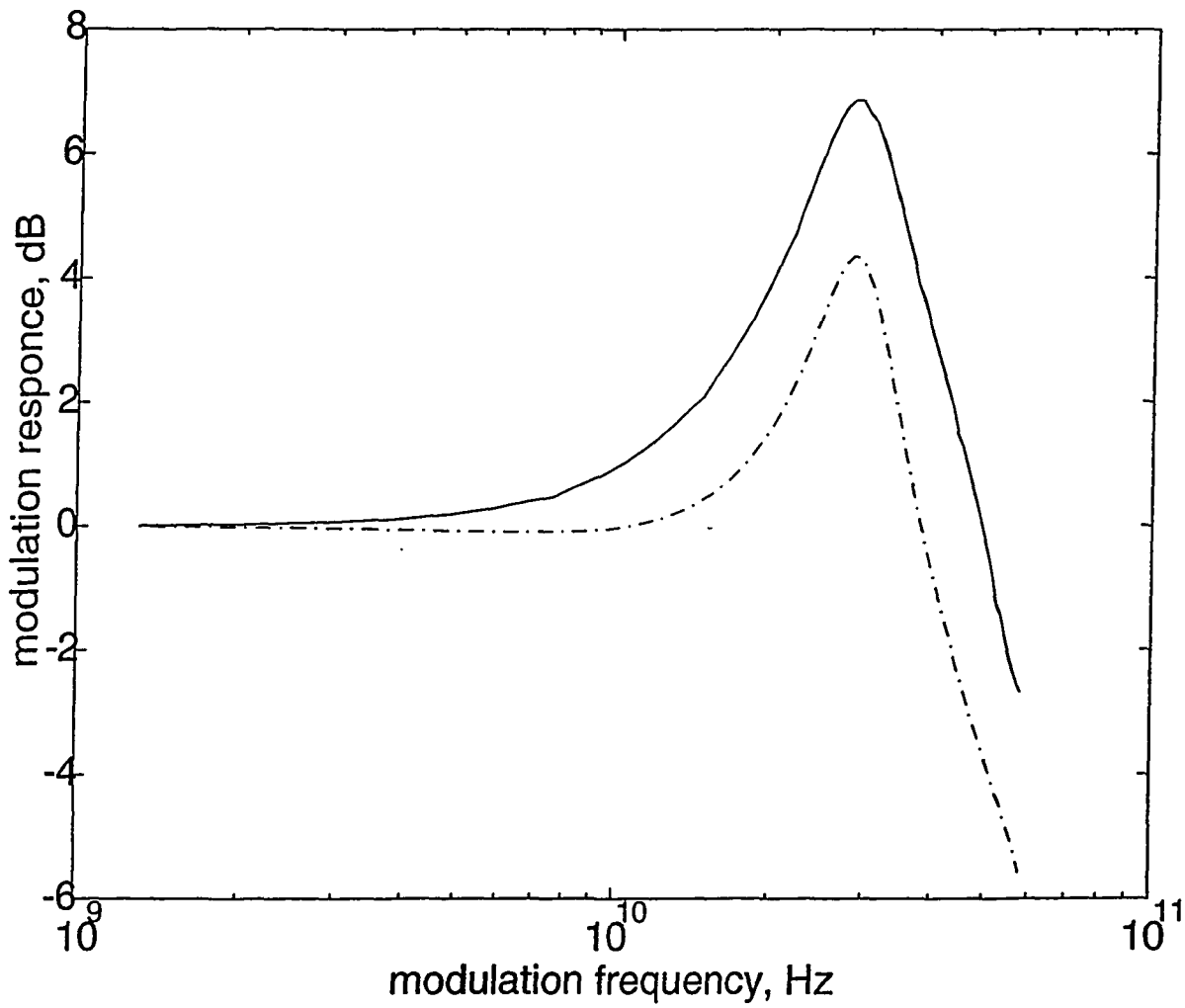

Figure 4.2a) Modulation response of the laser structure with hot phonon (solid line) and equilibrium phonon (dash-dotted line) models considered. Case A ($c_n = 2 \times 10^{13} s{-}1$).

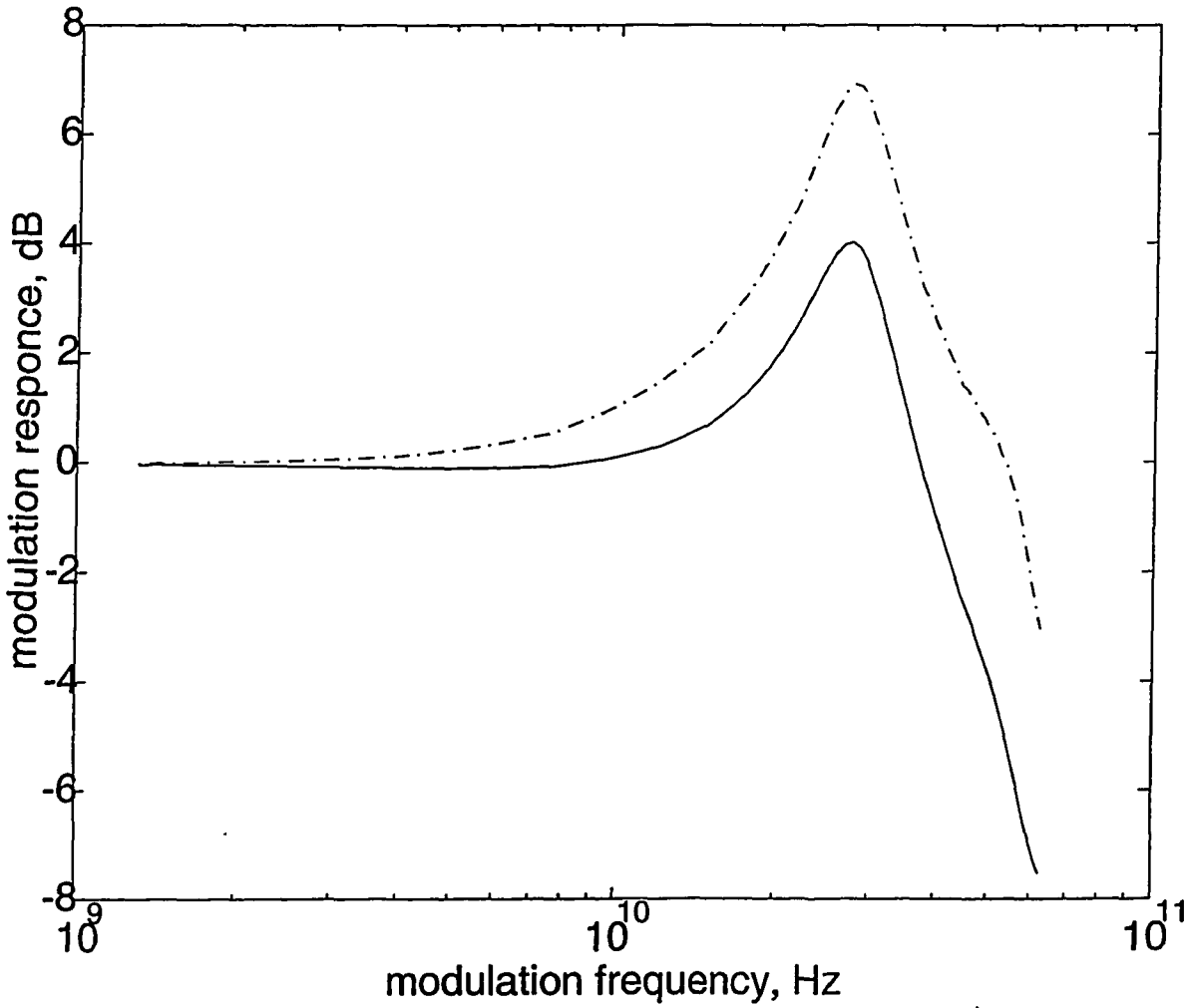

Figure 4.2b) Modulation response of the laser structure with hot phonon (solid line) and equilibrium phonon (dash-dotted line) models considered. Case B ($c_n = 1 \times 10^{12} s{-}1$).

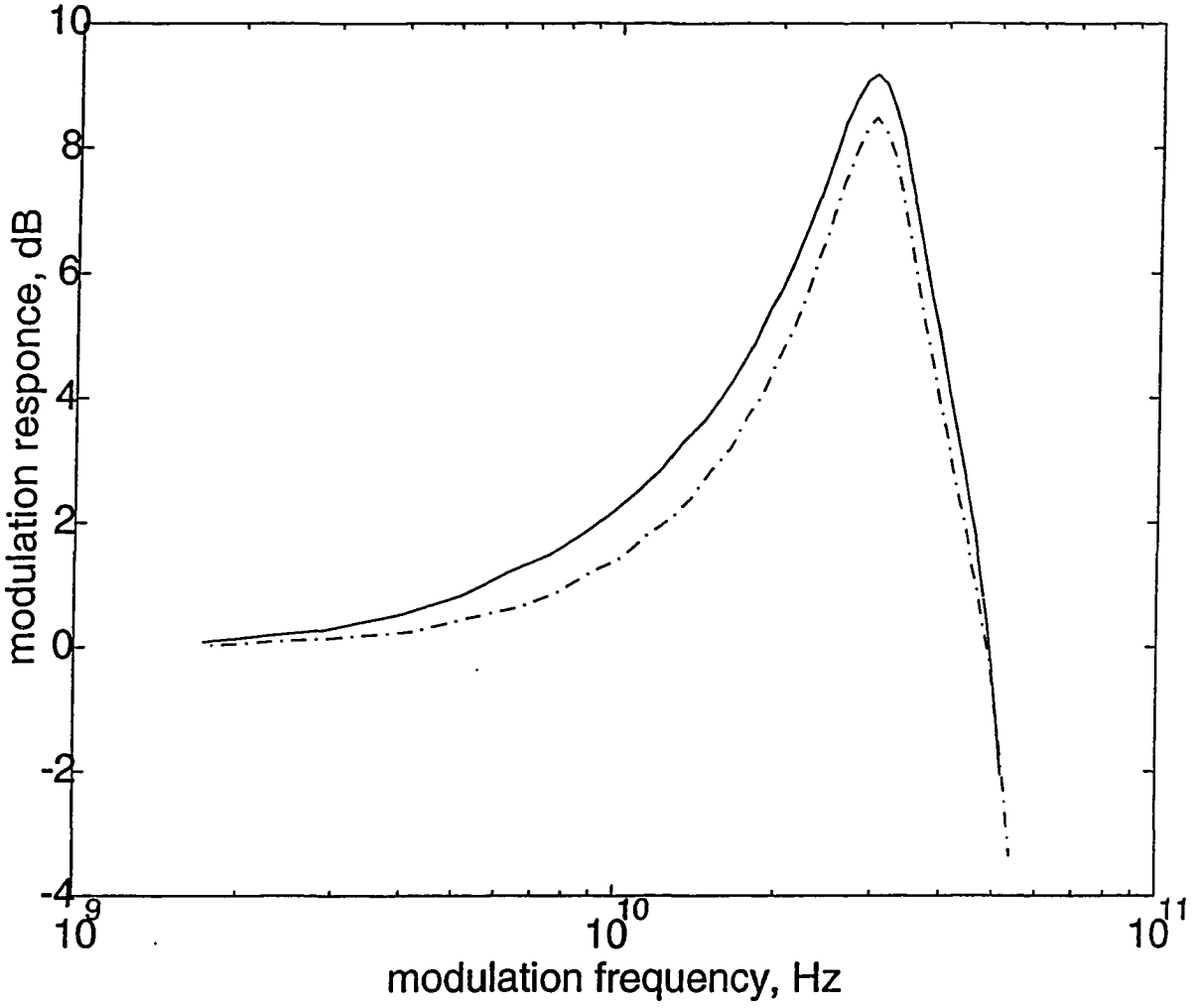

Figure 4.2c) Modulation response of the laser structure with hot phonon (solid line) and equilibrium phonon (dash-dotted line) models considered. Case C ($c_n = 4 \times 10^{12} s{-}1$).

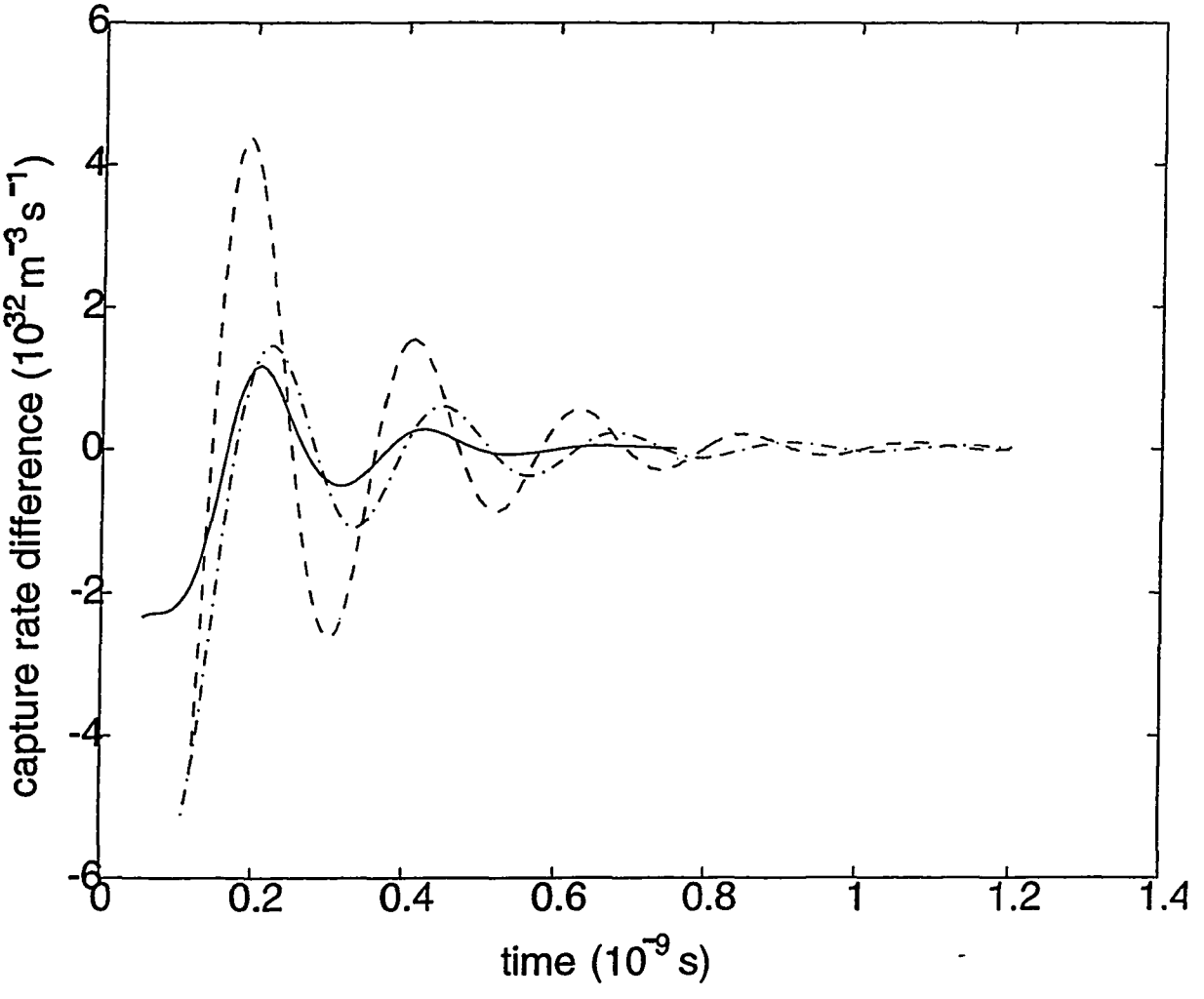

Figure 4.3 The difference in the net capture rate between the hot phonon and equilibrium phonon model step response calculations for Case A (dashed line), Case B (dash-dotted line) and Case C (solid line).

the one without, plotted on the time scale of the transient step response simulation. We see that in the simulation corresponding to case C the net capture rate in the thermal equilibrium phonon simulation is very close to that of the hot phonon simulation. In case B, the hot phonon rate is consistently below the equilibrium phonon rate, while in case A the hot phonon rate exceeds the equilibrium phonon rates for significant time intervals. Of course, this merely confirms the well-known [13, 31] and logically consistent positive correlation between the increase in the net capture rate and the improvement of modulation bandwidth. (The physical explanation for this correlation is still, however, a subject of discussion. See, for example, Grupen's study of the effect of diffusion capacitance related to wasted current on the modulation response [49]). The results shown in Fig. 4.3, however, are not easy to explain (or predict) analytically. Indeed, it is the very complicated relationship between the carrier, phonon, and capture rate dynamics which necessitate the detailed self-consistent simulation. As expected from Eq. (4.9), both rates – capture and emission – are enhanced as the result of nonequilibrium phonon inclusion in all three cases. However, the relative rate increases in the two models differ from case to case, making the **net** capture rates in the hot phonon model greater or less than the corresponding equilibrium phonon rates, depending on the carrier capture coefficient used.

4.4 Conclusion

Depending on the carrier capture coefficient in the quantum wells, we have found that the LO optical phonon scattering may either enhance or hurt the QW laser modulation

bandwidth. Since there are methods (such as the QW doping) which can affect the hot phonon population, it is important to know what the effect of hot phonons is in any particular case. For the purpose of simulation, this underscores the importance of better models for determining more precisely the carrier capture coefficient.

CHAPTER 5

CONCLUSIONS

The assumption of overall charge neutrality is so natural that using it as a fundamental assumption in laser threshold modeling was never challenged. We showed, however, that for very thin QW active regions, this constraint is no longer valid. The n/p ratios, much different from unity, were obtained for intrinsic quantum wells by modulation doping. It was further shown that while the increase of n over p caused the threshold current to rise, the increase of p over n resulted in the lowering of threshold current. Finally, the effect of threshold current dependence on the n/p ratio has been explained entirely in terms of the asymmetry in the conduction and valence band effective masses.

We developed a theoretical model for threshold current analysis of lasers that did not depend on parameters such as the cavity length, which are ill-defined for the Vertical Cavity Surface Emitting Lasers (VCSELs). We have shown the equivalence of this model with the Fabry-Perot model in the case of conventional edge-emitting semiconductor lasers, and in the particular case of VCSEL lasing. In a general analysis of VCSELs, however, when the lasing at the resonant peak frequency is not assumed, our model is shown to be better suited for analysis and simulation.

Finally, we investigated the effect of nonequilibrium phonons on the high frequency modulation response of semiconductor lasers in the context of self-consistent microscopic device simulation. It was shown that, unlike previously believed, it may be possible for nonequilibrium phonons to *improve* the net carrier capture into the quantum well, and thus increase the modulation bandwidth.

LIST OF REFERENCES

[1] H.C. Casey and M.B. Panish, Heterostructure Lasers, Parts A and B, Academic Press, Inc, Harcourt Brace Jovanovich, Publishers, 1978.

[2] G.P. Agrawal and N.K. Datta, Long-Wavelength Semiconductor Lasers, Van Nostrand Reinhold Co., 1986.

[3] H.F. Lockwood, H. Kressel, H.S. Sommers, and F.Z. Hawrylo, Appl. Phys. Lett. **17**, 499 (1970).

[4] N. Holonyak, R.M. Kolbas, R.D. Dupius, and P.D. Dapkus, IEEE J. Quantum Electron. **QE-16**, 170 (1980).

[5] N. Holonyak, R.M. Kolbas,W.D. Laidig, B.A. Vojak, K. Hess, R.D. Dupius, and P.D. Dapkus, J. Appl. Phys. **51**, 1328 (1980).

[6] Y. Arakawa and H. Sakaki, Appl. Phys. Lett. **40**, 939 (1982).

[7] Y. Arakawa, K. Vahala, and A. Yariv, Appl. Phys. Lett. **45**, 950 (1984).

[8] J. Cibert, P.M. Petroff, G.J. Dolan, S.J. Pearton, A.C. Gossard, and J.H. English, Appl. Phys. Lett. **49**, 1275 (1986).

[9] E. Yablonovich and E.O. Kane, J. Lightwave Tech. **LT-4**, 504 (1986).

[10] M.D. Camras, J.M. Brown, N. Holonyak, M.A. Nixon, R.W Kaliski, M.J. Ludowise, W.T. Dietze, and C.R. Lewis, J. Appl. Phys. **54**, 6183 (1983).

[11] G.D. Sanders and Y.-C. Chang Phys. Rev. B **32**, 4282 (1985).

[12] R.S. Geels, S.W. Corzine, J.W. Scott, D.B. Young, and L.A. Coldren, IEEE Photon. Tech. Lett. **2**, 234 (1990).

[13] K.Y. Lau, "Ultralow Threshold Quantum Well Lasers," in Quantum Well Lasers, Academic Press, Inc., P.S.Zory editor, 236 (1993).

[14] M. Grupen, G. Kosinovsky, and K. Hess, Proceed. IEEE Electron. Dev. Meetings (1993).

[15] H. Shichijo, R.M. Kolbas, N. Holonyak, R.D. Dupius, and P.D. Dapkus, Solid State Commun. **27**, 1029 (1978).

[16] J.Y. Tang, K. Hess, N. Holonyak, J.J. Coleman, and P.D. Dapkus, J. Appl. Phys. **53**, 6043 (1982).

[17] J.A.Brum and G. Bastard, Phys. Rev. B **33**, 1420 (1986).

[18] S.V. Kozyrev and A.Y. Shik, Sov. Phys. Semicond. **19**, 1024 (1986).

[19] P.W.M. Blom, R.F. Molls, J.E.M. Haverkort, M.R. Leys, and J.H. Wolter, Superlatt. and Microstruct. **7**, 319 (1990).

[20] P. Sotirelis and K. Hess, Phys. Rev. B **49**, 7543 (1994).

[21] J. Shah, Solid-State Electron. **31**, 43 (1978).

[22] K. Hess, N. Holonyak, W.D. Laidig, B.A. Vojak, J.J. Coleman, and P.D. Dapkus, Solid State Commun. **34**, 749 (1980).

[23] C.L. Collins and P.Y. Yu, Phys. Rev. B **30**, 4501 (1984).

[24] A.K. Sood, J. Menendez, M. Cardona, and K. Ploog, Phys. Rev. Lett. **54**, 2111 (1985).

[25] J.A. Kash, J.C. Tsang, and J.M. Hvam, Phys. Rev. Lett. **54**, 2151 (1985).

[26] J.A. Kash, J.M. Hvam, J.C. Tsang, and T. F. Kuech, Phys. Rev. B **38**, 5776 (1988).

[27] K.T. Tsen, R.P. Joshi, D.K. Ferry, and H. Morkoc, Phys. Rev. B **39**, 1446 (1989).

[28] D. Kim and P.Y. Yu Phys. Rev. Lett. **64**, 946 (1990).

[29] D. Kim and P.Y. Yu Phys. Rev. B **43**, 2210 (1991).

[30] L.F. Lester and B.K. Ridley, J. Appl. Phys. **72**, 2579 (1992).

[31] C.Y. Tsai, L.F. Eastman, and Y.H. Lo, Appl. Phys. Lett. **63**, 3408 (1993).

[32] K. Hess, B. A Vojak, N. Holonyak, Jr., R. Chin and P. D. Dapkus, Solid-St. Electron. **23**, 585 (1980).

[33] Y. Arakawa and A. Yariv, IEEE J. Quantum Electron. **QE-21**, 1666 (1985).

[34] Akira Sugimura, IEEE J. Quantum Electron. **QE-20**, 336 (1984).

[35] S. R. Chinn, P. S. Zory and A. R. Reisinger, IEEE J. Quantum Electron. **24**, 2191 (1988).

[36] D. P. Wilt and A.Yariv, IEEE J. Quantum Electron. **QE-17**, 1941 (1981).

[37] G. H. Song, K. Hess, T. Kerkhoven and U.Ravaioli, European Trans. Telecom. Related Tech. **1**, 375 (1990).

[38] S. Seki, M. Tomizawa, K. Yokoyama and Y. Yoshii, Tech. Dig. Int. Electron Device Meetings (1988).

[39] M. Grupen and K. Hess, Proceed. SPIE's OE/LASE Conference (1994).

[40] G.A. Kosinovsky, M.S. Thesis, University of Illinois at Urbana-Champaign, 1990.

[41] B. Tell, K.F. Brown-Goebeler, and R.E Leibenguth, IEEE Photon. Tech. Lett. **4**, 521 (1992).

[42] D.G. Deppe, Appl. Phys. Lett. **57**, 1721 (1990).

[43] T. Baba, T. Hamano, F. Koyama, and K. Iga, IEEE Journ. Quant. Elect. **27**, 1024 (1991).

[44] G. Börk, S. Machida, Y. Yamamoto, and K. Igeta Phys. Rev. A **44**, 669 (1991).

[45] J.W. Scott, S.W. Corzine, D.B. Young, and L.A. Coldren, Appl. Phys. Lett. **62**, 1050 (1993).

[46] J.W. Scott, R.S. Geels, S.W. Corzine, and L.A. Couldren, IEEE Journ. Quant. Elect. **29**, 1295 (1993).

[47] L.F. Register, R. Baca, G.A. Kosinovsky, M. Grupen, and K. Hess, to be published in Appl. Phys. Lett.

[48] N.W. Ashcroft and N.D. Mermin, Solid State Physics, W.B. Saunders Co., 466 (1976).

[49] M. Grupen and K. Hess, to be published in Appl. Phys. Lett.

VITA

Gregory Alexander Kosinovsky was born in Bobruysk, USSR (presently Belarus), on July 28, 1966. He emigrated with his family from the USSR in 1980, and went to high school in Omaha, Nebraska. He received the B.S. degree in Electrical Engineering with Highest Honors from the College of Engineering at the University of Illinois at Urbana-Champaign in May 1988, and the M.S. degree in Electrical Engineering in July 1990, from UIUC. He enrolled in the Ph.D. program at the University of Illinois at Urbana-Champaign in 1990.